Molecular Dynamics Modeling of the Structures and Binding Energies of α-Nickel Hydroxides and Nickel−Aluminum Layered Double Hydroxides Containing Various Interlayer Guest Anions

Hui Li and Jing Ma*

School of Chemistry and Chemical Engineering, Institute of Theoretical and Computational Chemistry, Key Laboratory of Mesoscopic Chemistry of MOE, Nanjing University, Nanjing, 210093, P.R. China

David G. Evans, Tong Zhou, Feng Li, and Xue Duan

Key Laboratory of Science and Technology of Controllable Chemical Reactions, Ministry of Education, Beijing University of Chemical Technology, Beijing 100029, P.R. China

Received April 13, 2006. Revised Manuscript Received June 10, 2006

Molecular dynamics (MD) simulations of β-Ni(OH)$_2$, α-Ni(OH)$_2$, and Ni/Al-layered double hydroxides (LDHs) have been performed in order to study structures and binding energies of the materials containing various anions such as CO_3^{2-}, SO_4^{2-}, OH^-, F^-, Cl^-, Br^-, and NO_3^-. We propose a modified force field of the cff91 form with the introduction of a double-well potential for describing oxygen−metal−oxygen angle bending. New parameters for describing the Ni−O bond and some refined nonbond parameters are suggested. The structural parameters of β-Ni(OH)$_2$, α-Ni(OH)$_2$, and Ni/Al-LDHs obtained with the modified force field are in good agreement with experimental values. For NO_3^- and SO_4^{2-} contained LDHs, the simulated results suggest several possible stacking modes of interlayer anions and water molecules. The stability of dehydrated β-Ni(OH)$_2$ has also been rationalized by the hydration energy of β-Ni(OH)$_2$. The relative binding energies of interlayer anions in α-Ni(OH)$_2$ and Ni/Al-LDHs decrease in the order $CO_3^{2-} > SO_4^{2-} > OH^- > F^- > Cl^- > Br^- > NO_3^-$, which is consistent with the observed relative ease of exchange of anions in the ion-exchange experiments employed for the synthesis of LDHs.

Introduction

Layered double hydroxides (LDHs), also known as hydrotalcite-like compounds, belong to an important class of readily synthesized compounds with great potential usages in fields of anion exchange and adsorption materials, carriers for drugs, antacids in medicine, electrode modifiers, catalysts, and catalyst supports.[1,2] LDHs have a host−guest structure, with stacks of positively charged mixed metal hydroxide layers, alternating with charge-balancing interlayer anions (the interlayer anions can be simple inorganic anions or much larger complex organic species).[3]

The structure of the layers in LDHs is analogous with that of brucite [Mg(OH)$_2$], consisting of metal cations surrounded approximately octahedrally by hydroxide anions.[4] These octahedral units form infinite layers, with the hydroxide ions sitting perpendicular to the layers. Such a brucite structure is adopted by many divalent metal hydroxides.

There has been considerable interest in hydroxide and LDH systems containing nickel. Nickel hydroxides have been widely studied[5−11] due to their usages in the active material of the positive electrode of nickel−cadmium batteries[5] and photochromic materials.[6] The electrocatalytic properties of Ni/Al LDHs are also of interest due to their potential applications in modified electrodes of amperometric sensors.[12] One polymorph of nickel hydroxide, β-Ni(OH)$_2$ **(1)**, is isostructural with Mg(OH)$_2$. In contrast to β-Ni(OH)$_2$, the structures of the other polymorphs of nickel hydroxide are still not well-characterized. α-Nickel hydroxide **(2)** is a less ordered material, which has an LDH-like structure with anions intercalated between the layers, even though there are no trivalent cations in the layers.[5−11] It has been suggested that the layers consist of $[Ni(OH)_{2-y-x}(H_2O)_x]^{(x+y)+}$ units with a net positive layer charge being created by hydroxyl vacancies ($x = 0$) or by protonation of hydroxyl groups ($y = 0$), or a combination of both.[10,11] It has also been suggested that, in some cases, for example, acetate may be coordinated to the nickel cations, giving neutral layers of the type $[Ni(OH)_{2-y}(Ac)_y]\cdot xH_2O$.[11] The basal spacing in α-Ni(OH)$_2$ (ca. 7.5 Å) is larger than that in β-Ni(OH)$_2$ (4.6 Å) as a

* To whom correspondence should be addressed. E-mail: majing@netra.nju.edu.cn.

(1) Cavani, F.; Trifirò, F.; Vaccari, A. *Catal. Today* **1991**, *11*, 173, and references therein.
(2) Rives, V., Ed. *Layered Double Hydroxides: Present and Future*, Nova Science Publishers: New York, 2001.
(3) Newman S. P.; Jones, W. *New J. Chem.* **1998**, *2*, 105.
(4) Wyckoff, R. W. G. *Crystal Structures*; Interscience: New York, 1960; Vol. 1.
(5) McEwen, R. S. *J. Phys. Chem.* **1971**, *75*, 1782.
(6) Zhou, T.; Li, F.; Evans, D. G.; Duan, X. Unpublished results.
(7) Le Bihan, S.; Figlarz, M. *J. Cryst. Growth* **1972**, *13*/*14*, 458.
(8) Ismail, J.; Ahmed, M. F.; Kamath, P. V.; Subbanna, G. N.; Uma, S.; Gopalakrishnan, J. *J. Solid State Chem.* **1995**, *114*, 550.
(9) Dixit, M.; Subbanna, G. N.; Kamath, P. V. *J. Mater. Chem.* **1996**, *6*, 1429.
(10) Kamath, P. V.; Therese, G. H. A. *J. Solid State Chem.* **1997**, *128*, 38.
(11) Poul, L.; Jouini, N.; Fiévet, F. *Chem. Mater.* **2000**, *12*, 3123.
(12) Scavetta E.; Berrettoni, M.; Giorgettti, M.; Tonelli, D. *Electrochim. Acta* **2002**, *47*, 2451.

10.1021/cm060867h CCC: $33.50
Published on Web 08/08/2006

consequence of the presence of interlayer anions in the former.

A key feature of LDHs and α-$Ni(OH)_2$ is their ability to undergo exchange of interlayer anions, which can be used to synthesize novel materials with different anions. It has been demonstrated that the affinity of the layers toward monovalent anions follows an empirical order $OH^- > F^- > Cl^- > Br^- > NO_3^-$.[3,13] The affinity for divalent anions such as CO_3^{2-} and SO_4^{2-} is higher than that for monovalent anions.[3] The variations in charge density as well as the shape of anions are presumably responsible for the relative ease of ion exchange. To date, however, there have been few attempts to present a systematic description of the variation in affinity of these materials containing different anions.

To understand such phenomena, detailed knowledge of both the structure of metal hydroxide layers and the packing modes of interlayer anions and water molecules is required. Unfortunately, experimental characterizations of the interlayers, surface regions, and even the detailed structure of the layers are difficult.[1] For instance, because of structural disorder and small crystallite size, X-ray diffraction can provide only limited information.[14] Other spectroscopic methods, such as multinuclear NMR, can also provide some information about these compounds.[15] Many of the fine details of the structure, such as the degree of ordering of metal cations within the layers, the stacking motif of the layers, and the arrangement of anions and water molecules in the highly disordered interlayer regions are not fully understood. Even accurate determination of the interlayer water content is difficult because of the strong interaction between water molecules and particle surfaces.[1,16]

With recent advances in computational software and hardware, theoretical calculations are now able to extend the scope of study of these materials beyond experimental observations. Although some density functional theory (DFT) studies of Mg/Al LDHs have been reported,[17,18] it is difficult to use such quantum mechanical calculations in a comparative study of a range of LDHs containing various interlayer anions because of the complexity of their structures. Molecular dynamics (MD) simulations within the framework of molecular mechanics (MM) can provide useful information about the structure and dynamical characteristics of these materials. There have been a number of MD studies of Mg/Al-LDHs reported in the literature,[16,19−29] which have provided comprehensive pictures of their structures. Here, we present a systematic MD study on β-$Ni(OH)_2$ **(1)**, α-$Ni(OH)_2$ **(2)**, and Ni/Al-LDHs **(3)** containing various kinds of interlayer anions: NO_3^- **(2a, 3a, 3h)**, Br^- **(2b, 3b)**, Cl^- **(2c, 3c)**, F^- **(2d, 3d)**, OH^- **(2e, 3e)**, SO_4^{2-} **(2f, 3f, 3i)**, and CO_3^{2-} **(2g, 3g)**, with an emphasis on understanding the relative anion affinity in LDHs. A modified force field based on the cff91 form[30] is proposed for the description of β-$Ni(OH)_2$ **(1)**, α-$Ni(OH)_2$ **(2)**, and Ni/Al-LDHs **(3)**. Our results provide not only important insight into the structure of the metal hydroxide layers and the arrangement of interlayer anions but also the relative binding energies of different anions with the layers. The interactions between host metal hydroxide layers and guest interlayer anions and the origin of the relative affinity of interlayer anions are addressed in the present work.

Computational Details

A. Model Construction. The structure of LDHs has been investigated by means of both single-crystal diffraction data from mineral samples[31] and refinement of powder diffraction data from synthetic samples.[14] The structural models employed in our simulations are based on the structure of Mg/Al hydrotalcite obtained by a refinement of powder X-ray diffraction data using the Rietveld method,[14] in which the structure was refined in a rhombohedral unit cell with space group $R\bar{3}m$. We assume $R\bar{3}m$ symmetry for the initial configuration of the primary layers in our LDH models, in line with other MD simulations.[16]

In contrast to LDHs, where the structure is relatively well-defined, only some limited structural data from powder diffraction[5] and EXAFS[32] are available for α-$Ni(OH)_2$ phases. As noted above, they are poorly ordered materials, which have an LDH-like structure with anions intercalated between the layers. To simplify, the hydroxyl vacancies and protonation of hydroxyl groups are neglected in our simulations since we are mainly interested in the relative affinity of various anions for the α-$Ni(OH)_2$ layers. The Mg/Al hydrotalcite structure[14] is also used to construct the initial structure of α-$Ni(OH)_2$. Although the resulting models of α-$Ni(OH)_2$ are similar to Ni/Al-LDHs, we can survey the role of incorporated Al atoms in the mixed hydroxide layers and the qualitative pictures of α-$Ni(OH)_2$ structure. In our model the nickel(II) cations in the layers are allocated an enhanced positive charge in order to balance the negative charge of the interlayer anions. The simulated supercell of α-$Ni(OH)_2$ contains a total of 20 crystallographic unit cells, $4 \times 5 \times 1$ in the *a*-, *b*-, and *c*-directions, respectively. Thus, every octahedral layer has 20 Ni atoms and 40 OH groups. Each supercell contains 3 interlayers, consisting of 4

(13) Miyata, S. *Clays Clay Miner.* **1983**, *31*, 305.
(14) Bellotto, M.; Rebours, B.; Clause, O.; Lynch, J.; Bazin, D.; Elkaïm, E. *J. Phys. Chem.* **1996**, *100*, 8527.
(15) Hou, X.; Kirkpatrick, R. J.; Yu, P.; Moore, D.; Kim, Y. *Am. Mineral.* **2000**, *85*, 133.
(16) (a) Wang, J.; Kalinichev, A. G.; Kirkpatrick, R. J.; Hou, X. *Chem. Mater.* **2001**, *13*, 145. (b) Numar, P. P.; Kalinichev, A. G.; Kirkpatrick, R. J. *J. Phys. Chem. B* **2006**, *110*, 3841.
(17) Greenwell, H. C.; Stackhouse, S.; Coveney, P. V.; Jones, W. *J. Phys. Chem. B* **2003**, *107*, 3476.
(18) Sato, H.; Morita, A.; Ono, K.; Nakano, H.; Wakabayashi, N.; Yamagishi, A. *Langmuir* **2003**, *19*, 7120.
(19) Aicken, A. M.; Bell, I. S.; Coveney, P. V.; Jones, W. *Adv. Mater.* **1997**, *6*, 496.
(20) Teppen, B. J.; Rasmussen, K.; Bertsch, P. M.; Miller, D. M.; Schäfer, L. *J. Phys. Chem. B* **1997**, *101*, 1579.
(21) Newman, S. P.; Williams, S. J.; Coveney, P. V.; Jones, W. *J. Phys. Chem. B* **1998**, *102*, 6710.
(22) Cygan, R. T.; Liang, J. J.; Kalinichev, A. G. *J. Phys. Chem. B* **2004**, *108*, 1255.
(23) Newman, S. P.; Di Cristina, T.; Coveney, P. V.; Jones, W. *Langmuir* **2002**, *18*, 2933.
(24) Fogg, A. M.; Rohl, A. L.; Parkinson, G. M.; O'Hare, D. *Chem. Mater.* **1999**, *11*, 1194.
(25) Kalinichev, A. G.; Kirkpatrick, R. J.; Cygan, R. T. *Am. Mineral.* **2000**, *85*, 1046.
(26) Hou, X.; Kalinichev, A. G.; Kirkpatrick, R. J. *Chem. Mater.* **2002**, *14*, 2078.
(27) Kalinichev, A. G.; Kirkpatrick, R. J. *Chem. Mater.* **2002**, *14*, 3539.
(28) Wang, J.; Kalinichev, A. G.; Amonette, J. E.; Kirkpatrick, R. *J. Am. Mineral.* **2003**, *88*, 398.
(29) Kim, N.; Kim, Y.; Tsotsis, T. T.; Sahimi, M. *J. Chem. Phys.* **2005**, *122*, 214713.
(30) Maple, J. R.; Hwang, M.-J.; Stockfisch, T. P.; Dinur, U.; Waldman, M.; Ewig, C. S.; Hagler, A. T. *J. Comput. Chem.* **1994**, *15*, 162.
(31) Taylor, H. F. W. *Miner. Magn.* **1973**, *39*, 377.
(32) Pandya, K. I.; O'Grady, W. E.; Corrigan, D. A.; McBreen, J.; Hoffman, R. W. *J. Phys. Chem.* **1990**, *94*, 21.

Table 1. Molecular Formulas of the Model Used in Simulations

LDH model	interlayer anion	molecular formula
β-Ni(OH)$_2$ **(1)**		$Ni_{20}(OH)_{40}(H_2O)_x$ ($x = 0-20$)
α-Ni(OH)$_2$ **(2)**		
NO_3^-−α-Ni(OH)$_2$ **(2a)**	NO_3^-	$Ni_{20}(OH)_{40}(NO_3)_4(H_2O)_9$
Br^-−α-Ni(OH)$_2$ **(2b)**	Br^-	$Ni_{20}(OH)_{40}Br_4(H_2O)_{15}$
Cl^-−α-Ni(OH)$_2$ **(2c)**	Cl^-	$Ni_{20}(OH)_{40}Cl_4(H_2O)_{15}$
F^-−α-Ni(OH)$_2$ **(2d)**	F^-	$Ni_{20}(OH)_{40}F_4(H_2O)_{15}$
OH^-−α-Ni(OH)$_2$ **(2e)**	OH^-	$Ni_{20}(OH)_{40}(OH)_4(H_2O)_{15}$
SO_4^{2-}−α-Ni(OH)$_2$ **(2f)**	SO_4^{2-}	$Ni_{20}(OH)_{40}(SO_4)_3(H_2O)_{10}$
CO_3^{2-}−α-Ni(OH)$_2$ **(2g)**	CO_3^{2-}	$Ni_{20}(OH)_{40}(CO_3)_3(H_2O)_{10}$
Ni/Al-LDHs **(3)**		
NO_3^-−Ni/Al-LDH **(3a)**	NO_3^-	$Ni_{18}Al_6(OH)_{48}(NO_3)_6(H_2O)_{12}$
Br^-−Ni/Al-LDH **(3b)**	Br^-	$Ni_{18}Al_6(OH)_{48}Br_6(H_2O)_{18}$
Cl^-−Ni/Al-LDH **(3c)**	Cl^-	$Ni_{18}Al_6(OH)_{48}Cl_6(H_2O)_{18}$
F^-−Ni/Al-LDH **(3d)**	F^-	$Ni_{18}Al_6(OH)_{48}F_6(H_2O)_{18}$
OH^-−Ni/Al-LDH **(3e)**	OH^-	$Ni_{18}Al_6(OH)_{48}(OH)_6(H_2O)_{18}$
SO_4^{2-}−Ni/Al-LDH **(3f)**	SO_4^{2-}	$Ni_{18}Al_6(OH)_{48}(SO_4)_3(H_2O)_{12}$
CO_3^{2-}−Ni/Al-LDH **(3g)**	CO_3^{2-}	$Ni_{18}Al_6(OH)_{48}(CO_3)_3(H_2O)_{12}$
NO_3^-−Ni/Al-LDH **(3h)**	NO_3^-	$Ni_{12}Al_6(OH)_{36}(NO_3)_6(H_2O)_9$
SO_4^{2-}−Ni/Al-LDH **(3i)**	SO_4^{2-}	$Ni_{12}Al_6(OH)_{36}(SO_4)_3(H_2O)_{24}$

monovalent anions (NO_3^-, Br^-, Cl^-, F^-, or OH^-) or 3 divalent anions (SO_4^{2-} or CO_3^{2-}) and a predetermined number of water molecules based on the experimentally determined stoichiometries of α-Ni(OH)$_2$ containing NO_3^- **(2a)**, Cl^- **(2c)**, and SO_4^{2-} **(2f)**.[10] Then, Cl^- is changed to Br^-, F^-, and OH^- respectively to obtain other α-Ni(OH)$_2$ models containing Br^- **(2b)**, F^- **(2d)**, and OH^- **(2e)**. In the same way, SO_4^{2-} is changed to CO_3^{2-} to afford CO_3^{2-}-contained α-Ni(OH)$_2$ model **(2g)**. In the reported X-ray structure refinement of Mg/Al hydrotalcite, the positions of both the interlayer anions and water molecules were preassigned at the midpoint of the interlayer space along the *c*-axis.[14] Like what has been done in previous works,[16] anions and water molecules are initially set at random positions within the interlayer space in our simulations.

For Ni/Al-LDHs **(3)**, the ratio Ni/Al is chosen to be 3:1, as is commonly observed in LDHs.[1] Al atoms are randomly distributed in the hydroxide sheets, subjected to the constraint of avoiding the presence of two neighboring AlO_6 octahedra. A supercell of $4 \times 6 \times 1$ is adopted in each simulation model, and all the initial structures are constructed on the basis of the structure of Mg/Al hydrotalcite.[14] The same number of interlayer water molecules are added in α-Ni(OH)$_2$ **(2)** containing Br^-, Cl^-, F^-, OH^-, CO_3^{2-}, and SO_4^{2-} **(3f)**, while the interlayer water content of NO_3^--Ni/Al-LDH **(3a)** is taken from the experimental observation.[10] To study the packing motifs of NO_3^- and SO_4^{2-} anions, two other models are used: one is an Ni_2Al LDH containing NO_3^- **(3h)**[33] and the other is an Ni_2Al-LDH containing SO_4^{2-} **(3i)**, whose stoichiometry is similar to that of the Fe(II−III) layered double hydroxysulfate green rust two.[34] The formulas of α-Ni(OH)$_2$ **(2)** and Ni/Al-LDHs **(3)** supercells are shown in Table 1.

B. Simulations. A modified cff91 force field[30,35] is employed in our MD simulations, with the force field parameters taken from the force field published by Teppen et al.[20] Hill and Sauer's force constants[36,37] for Al, O, and H are used for the bond-stretching and angle-bending terms, and they are coupled with new parameters. The torsion contribution is neglected. The nickel−oxygen bond stretching constant and nickel−oxygen−nickel bending constant are derived from the Raman spectrum of β-Ni(OH)$_2$.[38−41] A two-well potential[20]

$$E_{\text{bond}} = -k_2(\theta - \theta_0)^2 + k_4(\theta - \theta_0)^4 \quad (1)$$

is used for describing the oxygen−metal−oxygen angle-bending

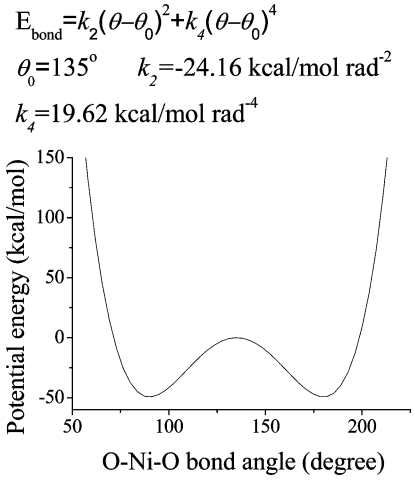

Figure 1. Two-well O−Ni−O angle-bending potential.[20]

potential so that the O−M−O angle, θ, displays two minima at 90° and 180° in order to maintain octahedral geometry, as shown in Figure 1.

Partial charges of layer atoms are initially assigned on the basis of Mulliken population analysis on the unit cell of β-Ni(OH)2 **(1)**,[42] which is optimized by periodic DFT[43,44] implemented in the Dmol^3 program of Cerius^2 software,[45] using the generalized gradient approximation (GGA)[46] including a double numeric basis set and polarized functions. The partial charges on the hydroxyl oxygen and hydrogen atoms are −0.795 and +0.393, respectively, and the charge on the Ni atom is +0.805. Partial charges of water molecules are directly taken from the CLAYFF force field,[22] and other parameters of water molecules are directly taken from the cff91 force field. It is necessary to test the performance of the used combination of parameters. From our MD simulation on liquid water in isothermal−isobaric (NPT) ensemble with the pressure set to be 0.1 MPa, and the temperature to 298 K, it can be found that the present parameters can reasonably reproduce the thermodynamic and structural properties of water, as shown in Table S1 (Supporting Information). The partial charges of interlayer anions are derived from natural bond orbital (NBO) population analysis[47] based on DFT calculations at the B3LYP[48,49]/6-31+G(d) level as implemented in Gaussian 03.[50] In α-Ni(OH)$_2$ **(2)** and Ni/ Al-LDHs **(3)**, the net positive charges are evenly distributed over each nickel atom. The partial charge of Al atoms (+1.68) in Ni/Al LDHs is taken from Teppen's force field directly.[20]

The Lennard-Jones 9-6 function form[30] of the cff91 force field is employed, with most of the van der Waals parameters coming from Teppen's force field.[20] Some repulsive and dispersive van

(33) Xu, Z. P.; Zeng, H. C. *J. Phys. Chem. B* **2001**, *105*, 1743.
(34) Simon, L.; François, M.; Refait, P.; Renaudin, G.; Lelaurain, M.; Génin, J.-M. R. *Solid State Sci.* **2003**, *5*, 327.
(35) Yu, C.-H.; Newton, S. Q.; Norman, M. A.; Schäfer, L.; Miller, D. M. *Struct. Chem.* **2003**, *14*, 175.
(36) Hill, J.-R.; Sauer, J. *J. Phys. Chem.* **1994**, *98*, 1238.
(37) Hill, J.-R.; Sauer, J. *J. Phys. Chem.* **1995**, *99*, 9536.
(38) Desilvestro, J.; Corrigan, D. A.; Weaver, M. J. *J. Phys. Chem.* **1986**, *90*, 6408.
(39) Kostecki, R.; McLarnon, F. *J. Electrochem. Soc.* **1997**, *144*, 485.
(40) Audemer, A.; Delahaye, A.; Farhi, R.; Sac-Epée, N.; Tarascon, J.-M. *J. Electrochem. Soc.* **1997**, *144*, 2614.
(41) Pascale, F.; Tosoni, S.; Zicovich-Wilson, C.; Ugliengo, P.; Orlando, R.; Dovesi, R. *Chem. Phys. Lett.* **2004**, *396*, 308.
(42) Greaves, C.; Thomas, M. A. *Acta Crystallogr. B* **1986**, *42*, 51.
(43) Delley, B. *J. Chem. Phys.* **1990**, *92*, 508.
(44) Delley, B. *J. Chem. Phys.* **2000**, *113*, 7756.
(45) *Cerius*^{2}, Version 3.5; Molecular Simulation Inc.: San Diego, CA, 1997.
(46) Perdew, J. P.; Wang, Y. *Phys. Rev. B: Condens. Matter* **1992**, *45*, 13244.
(47) Reed, A. E.; Curtiss, L. A.; Weinhold, F. *Chem. Rev.* **1988**, *88*, 899.
(48) Becke, A. D. *J. Chem. Phys.* **1993**, *98*, 5648.
(49) Lee, C.; Yang, W.; Parr, R. G. *Phys. Rev. B* **1988**, *37*, 785.

der Waals parameters of the metal hydroxide layer are reparametrized until they reproduce the crystal structure of β-Ni(OH)$_2$ **(2)**[40] with satisfactory accuracy. The van der Waals parameters of interlayer anions and water molecules are obtained directly from the cff91 force field.[28] The parameters used in our simulations are listed in Table 2.

Except for the periodic boundary conditions imposed on the simulation supercell, there are no additional symmetry constraints. The structure is treated as triclinic ($P1$ symmetry) and all cell parameters, a, b, c, α, β, and γ, are considered as independent variables during our MD simulations. For potential energy calculations, a "spline cutoff" method is used to calculate nonbonding van der Waals interactions, and Ewald summation is used to calculate long-range Coulombic interactions.[51] All simulations are performed in the isothermal−isobaric (NPT) ensemble with the pressure set to be 0.1 MPa and the temperature to 298 K. The temperature is controlled using the Andersen method,[52] and the pressure is controlled by the Parrinello-Rahman method.[53] The MD time step is 1.0 fs.

A 400-ps MD simulation of Cl$^-$-Ni/Al-LDH **(3c)** is also performed to test the sufficiency of the time scale in our simulations. The average structural parameters during different periods are listed in Table 3. The studied system can attain equilibration within a few picoseconds because of the small size and high rigidity of our systems. The 60-ps MD simulation is performed for each model. After a 20-ps equilibration period of each simulation, dynamic trajectories of the next 40 ps are recorded every 10 fs for statistical analysis.

Results and Discussion

A. Structure of β-Ni(OH)$_2$. The MD simulations reproduce the structure of β-Ni(OH)$_2$ **(1)**, yielding unit cell parameters of $a = b = 3.12$ Å and $c = 4.66$ Å comparable to experimental values ($a = b = 3.13$ Å and $c = 4.59$ Å).[42] The modified force field based on the cff91 form is able to give a proper Gaussian-shape distribution of bond length of the metal−oxygen bond, as shown in Figure 2, with the bond length populated around 2.06 Å, in good agreement with the experimental value of 2.07 Å.[42]

MD calculations on brucite[54] have indicated that the O−H bonds are, on average, perpendicular to the octahedral sheets with bifurcated and trifurcated hydrogen bonds between two hydroxide layers, consistent with neutron diffraction data.[55] Our simulations on β-Ni(OH)$_2$ **(1)** give similar results.

Table 2. Force Field Parameters for Molecular Dynamics of β-Ni(OH)$_2$, α-Ni(OH)$_2$, and Ni/Al-LDHs

Atom Type Description

ao	Al in octahedral coordination
nio	Ni in octahedral coordination
oh	O in the octahedral sheet, triply coordinated
ho	H in hydroxyl groups
o*	O in water molecule
hw	H in water molecule
Br	interlayer Br$^-$
Cl	interlayer Cl$^-$
F	interlayer F$^-$
oh*	O in interlayer OH$^-$ anions
ho*	H in interlayer OH$^-$ anions
nno3	N in interlayer NO_3^- anions
ono3	O in interlayer NO_3^- anions
sso4	S in interlayer SO_4^{2-} anions
oso4	O in interlayer SO_4^{2-} anions
cco3	C in interlayer CO_3^{2-} anions
oco4	O in interlayer CO_3^{2-} anions

Bond Stretching: $E_{ij} = k_2(r - r_0)^2 + k_3(r - r_0)^3 + k_4(r - r_0)^4$

i	j	r_0 (Å)	k_2 (kcal/(mol Å^2))	k_3 (kcal/(mol Å^3))	k_4 (kcal/(mol Å^4))
ao	oh	1.955	328.7	−341.0	2189.0
nio	oh	2.210	137.0	−261.0	218.2
oh	ho	0.965	532.5	−1282.9	2004.8
o*	hw	0.97	563.28	−1428.22	1902.12
oh*	ho*	0.97	563.28	−1428.22	1902.12
nno3	ono3	1.265	776.30	0	0
sso4	oso4	1.5300	505.94	0	0
cco3	oco3	1.234	711.35	−1543.9	1858.6

Angle Bending: $E_{ijk} = k_2(\theta - \theta_0)^2 + k_3(\theta - \theta_0)^3 + k_4(\theta - \theta_0)^4$

i	j	k	θ_0	k_2 (kcal/(mol rad^2))	k_3 (kcal/(mol rad^3))	k_4 (kcal/(mol rad^4))
hw	o*	hw	103.7	49.84	−11.60	−8.0
ao	oh	ao	109.5	195.5	48.9	185.3
nio	oh	nio	106.0	195.5	48.9	185.3
oh	ao	oh	135.0	−40.0	0.0	32.4
oh	nio	oh	135.0	−24.16	0.0	19.62
ao	oh	ho	118.0	44.0	−53.4	103.4
nio	oh	ho	118.0	44.0	−53.4	103.4
nno3	ono3	nno3	120.0	70.0	0	0
sso4	oso4	sso4	109.5	60.66	0	0
cco3	oco3	cco3	130.01	111.29	−52.339	−28.107

Nonbonded (1,2- and 1,3-Interactions Excluded):

$$E = \epsilon_{ij}\left[2\left(\frac{r_{ij}^0}{r_{ij}}\right)^9 - 3\left(\frac{r_{ij}^0}{r_{ij}}\right)^6\right] + 332.1\frac{q_i q_j}{r_{ij}},$$

$$\text{where } r_{ij}^0 = \left(\frac{r_i^6 + r_j^6}{2}\right)^{1/6},\ \epsilon_{ij} = 2\sqrt{\epsilon_i \epsilon_j}\,\frac{r_i^3 r_j^3}{\sqrt{r_i^6 + r_j^6}}$$

atom type	r (Å)	ϵ (kcal/ mol)	q
ao	6.2601	1.5767	1.68
nio	5.5601	1.5767	0.805
oh	1.9080	0.6740	−0.795
ho	1.0980	0.0130	0.393
hw	1.0980	0.0130	0.41
o*	3.6080	0.2740	−0.82
Br	4.3000	0.3600	−1.0
Cl	4.0000	0.4000	−1.0
F	3.3700	0.4000	−1.0
oh*	3.6080	0.2740	−1.395
ho*	1.0980	0.0130	0.395
cac1	3.9080	0.1200	0.759
cac2	4.0100	0.0540	−0.796
oac	3.5960	0.1670	−0.805
hac	2.9950	0.0200	0.216
nno3	4.0700	0.1340	0.684
ono3	3.5960	0.1670	−0.561
sso4	4.0270	0.0710	2.529
oso4	3.5960	0.1670	−1.132
cco3	3.9080	0.1200	0.931
oco4	3.5960	0.1670	−0.977

(50) Frisch, M. J.; Trucks, G. W.; Schlegel, H. B.; Scuseria, G. E.; Robb, M. A.; Cheeseman, J. R.; Montgomery, J. A.; Vreven, T., Jr.; Kudin, K. N.; Burant, J. C.; Millam, J. M.; Iyengar, S. S.; Tomasi, J.; Barone, V.; Mennucci, B.; Cossi, M.; Scalmani, G.; Rega, N.; Petersson, G. A.; Nakatsuji, H.; Hada, M.; Ehara, M.; Toyota, K.; Fukuda, R.; Hasegawa, J.; Ishida, M.; Nakajima, T.; Honda, Y.; Kitao, O.; Nakai, H.; Klene, M.; Li, X.; Knox, J. E.; Hratchian, H. P.; Cross, J. B.; Adamo, C.; Jaramillo, J.; Gomperts, R.; Stratmann, R. E.; Yazyev, O.; Austin, A. J.; Cammi, R.; Pomelli, C.; Ochterski, J. W.; Ayala, P. Y.; Morokuma, K.; Voth, G. A.; Salvador, P.; Dannenberg, J. J.; Zakrzewski, V. G.; Dapprich, S.; Daniels, A. D.; Strain, M. C.; Farkas, O.; Malick, D. K.; Rabuck, A. D.; Raghavachari, K.; Foresman, J. B.; Ortiz, J. V.; Cui, Q.; Baboul, A. G.; Clifford, S.; Cioslowski, J.; Stefanov, B. B.; Liu, G.; Liashenko, A.; Piskorz, P.; Komaromi, I.; Martin, R. L.; Fox, D. J.; Keith, T.; Al-Laham, M. A.; Peng, C. Y.; Nanayakkara, A.; Challacombe, M.; Gill, P. M. W.; Johnson, B.; Chen, W.; Wong, M. W.; Gonzalez, C.; Pople, J. A. *Gaussian 03*: Revision B.04; Gaussian, Inc.: Pittsburgh, PA, 2003.
(51) Karasawa, N.; Goddard, W. A., III. *J. Phys. Chem.* **1989**, *93*, 7320.
(52) Andersen, H. C. *J. Chem. Phys.* **1980**, *72*, 2384.
(53) Parrinello, M.; Rahman, A. *J. Appl. Phys.* **1981**, *52*, 7182.
(54) Wang, J.; Kalinichev, A. G.; Kirkpatrick, R. J. *Geochim. Cosmochim. Acta* **2004**, *68*, 3351.

Table 3. Simulated Structure during Different Periods in the 400 ps MD Simulation of the Cl^-−Ni/Al-LDH (3c)

time (ps)	α (deg)	β (deg)	γ (deg)	*a* (Å)	*b* (Å)	interlayer distance (Å)
0−5	90.1	89.9	60.0	12.24	18.36	7.77
5−10	90.1	90.0	60.0	12.23	18.36	7.77
10−15	90.3	89.9	60.0	12.23	18.36	7.76
15−20	90.2	89.9	60.0	12.23	18.35	7.74
20−50	90.2	89.9	60.0	12.22	18.35	7.75
50−100	90.2	89.9	60.0	12.23	18.35	7.76
100−400	90.2	89.9	60.0	12.23	18.35	7.76

Furthermore, in brucite and brucite-like structures such as LDHs, it is well-known that the MO_6 octahedra are compressed along the stacking axis[42] so that the local geometry around the metal is of D_{3d} symmetry, rather than O_h. In β-$Ni(OH)_2$, this leads to an increase in O···O and Ni···Ni distances parallel to the *ab* plane from 2.93 Å (calculated from an ideal O_h geometry) to 3.13 Å, with the O−M−O bond angles distorted to 97.9° and 82.1°, respectively, rather than a regular 90°.[42] This distortion has been discussed from a molecular orbital viewpoint.[56] In fact, the present simulation results on β-$Ni(OH)_2$ support that nearly all brucite-like hydroxides share a general trend in geometry distortions, which was suggested on the basis of the correlation between unit cell parameters and M−O distances.[57]

B. Hydration Energy of β-Ni(OH)$_2$. β-$Ni(OH)_2$ **(1)** is known to have the dry brucite structure without interlayer water molecules,[54] in contrast to wet structures of α-$Ni(OH)_2$ **(2)** and Ni/Al-LDHs **(3)**. An in-depth study on water molecules confined in nanopores between brucite (001) surfaces has demonstrated that the hydrophilic layer surfaces significantly influence the near-surface water structure.[54] To probe the reasons for the existence of a stable anhydrous structure, for β-$Ni(OH)_2$ **(1)**, 0−20 water molecules per interlayer have been successively put into the interlayer galleries of the studied models. Each model is simulated in an NPT ensemble. The potential energies are then recorded. It was found that the presence of the interlayer water molecules leads to an increase in the total potential energy of β-$Ni(OH)_2$. To estimate the increment in energy resulting from the addition of interlayer water molecules, the hydration energy $\Delta U_H(N)$ is defined as

$$\Delta U_H(N) = \frac{\langle U(N)\rangle - \langle U(0)\rangle - N\langle U_{H_2O}\rangle}{N} \qquad (2)$$

where $\langle U(N)\rangle$ is the average potential energy of wet β-$Ni(OH)_2$ with *N* water molecules in the interlayer galleries, $\langle U_{H_2O}\rangle$ is the average potential energies of a single water molecule, and $\langle U(0)\rangle$ is the average potential energy of dry β-$Ni(OH)_2$ **(1)** without water molecules in the interlayer.

Figure 3 shows that the hydration energy of β-$Ni(OH)_2$ **(1)** is positive for all values of *N*, implying that anhydrous β-$Ni(OH)_2$ is more stable than hydrated β-$Ni(OH)_2$, consistent with experimental observations. Although the introduction of interlayer water molecules may cause favorable interactions between hydroxide layers and water molecules, the concomitant expansion in interlayer spacing (as shown in Figure 3b) results in a significant decrease in the electrostatic interactions between adjacent sheets.

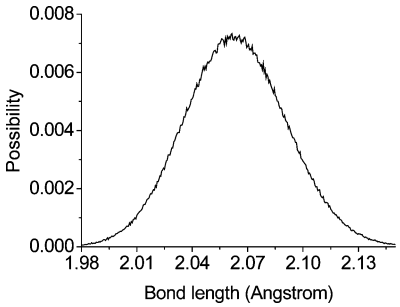

Figure 2. Distribution of Ni−O distance in β-$Ni(OH)_2$ obtained from NPT-ensemble MD simulations (298 K, 1 atm).

C. Structure of α-Ni(OH)$_2$ and Ni/Al LDHs. The MD simulations provide detailed information about the structures of α-$Ni(OH)_2$ **(2)** and Ni/Al-LDHs **(3)**. During the simulations, the layers of metal hydroxide octahedra are observed to maintain rigidity. Tables 4 and 5 show geometries for α-$Ni(OH)_2$ **(2)** and Ni/Al-LDHs **(3)**, as well as those of β-$Ni(OH)_2$ **(1)** for comparison purposes. The average values of the essentially identical *a*- and *b*-axis lengths of the unit cell are about 3.10 Å in α-$Ni(OH)_2$ systems **(2)** and about 3.06 and 3.04 Å in the Ni/Al-LDHs **(3)** with Ni/Al = 3 and 2, respectively, slightly smaller than 3.12 Å in β-$Ni(OH)_2$ **(1)**. The values of *a* parameter (equal to the average O···O distance) are in good agreement with experimental data from XRD (β-$Ni(OH)_2$: 3.13 Å;[5] α-$Ni(OH)_2$: 3.10 Å;[10] Ni_3Al-LDHs: 3.05 Å;[58] Ni_2Al-LDHs: 3.03 Å[58]). As is well-known for LDHs,[1] the experimental value of *a* parameter decreases with decreasing Ni/Al ratio, probably due to the larger radius of the Ni^{2+} cation than that of the Al^{3+}. The same trend is reproduced in our calculations. The average Ni−O bond lengths of 2.06 Å in β-$Ni(OH)_2$ **(1)** and 2.04−2.05 Å in α-$Ni(OH)_2$ **(2)** and Ni/Al-LDHs **(3)** are also in good agreement with experimental XAFS data (β-$Ni(OH)_2$: 2.07 Å; α-$Ni(OH)_2$: 2.05 Å; Ni/Al-LDHs: 2.05 Å).[59] As expected, the Al−O bond length (1.91 Å) in Ni/Al-LDHs **(3)** is shorter than that of Ni−O (2.05 Å).

The interlayer distance *d* increases with the increasing number and volume of the interlayer anions. Although the γ angles of the supercells are maintained at 60°, in fact, the energy minimization drives the interlayer molecules and sheets to more favorable positions, and consequently hydroxide layers glide, causing the change from the rhombohedral supercell to a triclinic one.

Furthermore, it can be seen from our simulations that the metal−oxygen bond length shows a correlation with the charge carried by the interlayer anions. The nickel−oxygen bond lengths decrease from 2.06 Å in β-$Ni(OH)_2$ **(1)** to 2.05 Å in α-$Ni(OH)_2$ **(2)** and Ni/Al-LDHs **(3)** containing monovalent interlayer anions, NO_3^- **(2a, 3a)**, Br^- **(2b, 3b)**, Cl^-

(55) Desgranges, L.; Calvarin, G.; Chevrier, G. *Acta Crystallogr. B* **1996**, *52*, 82.
(56) Peterson, R. C.; Hill, R. J.; Gibbs, G. V. *Can. Mineral.* **1979**, *17*, 703.
(57) Brindley, G. W.; Kao, C. C. *Phys. Chem. Miner.* **1984**, *10*, 187.
(58) Hernandez-Moreno, M. J. H.; Ulibarri, M. A.; Rendon, J. L.; Serna, C. J. *Phys. Chem. Miner.* **1985**, *12*, 34.
(59) Scheinost, A. C.; Ford, R. G.; Sparks, D. L. *Geochim. Cosmochim. Acta* **1999**, *63*, 3193.

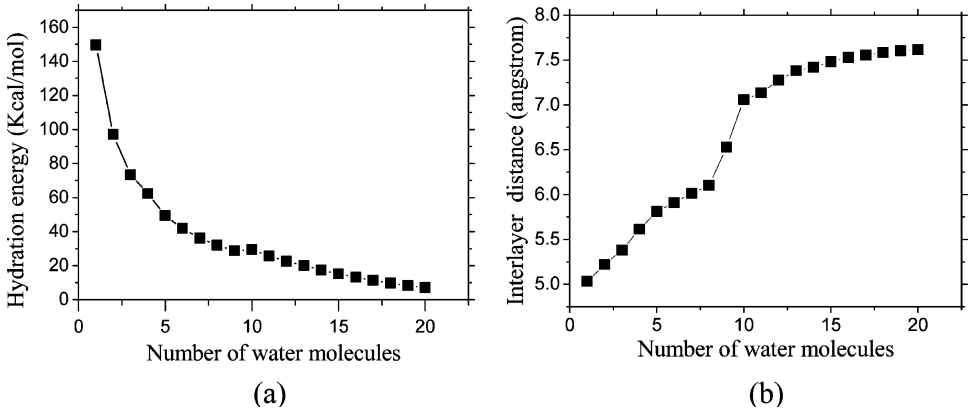

Figure 3. Variations of (a) average hydration energies (in kcal/mol) and (b) interlayer spacing (in Å) as a function of the number of interlayer water molecules per simulated cell, x, in $Ni_{20}(OH)_{40}{\cdot}xH_2O$, $x = 1-20$.

Table 4. Simulated Structures of β-Ni(OH)$_2$ (1) and α-Ni(OH)$_2$ (2) Models

	a (Å)	*b* (Å)	Ni−O (Å)	O···O (Å)	interlayer distance (Å)
β-$Ni(OH)_2$ **(1)**	12.48	15.60	2.06	3.12	4.66
$Ni_{20}(OH)_{40}(NO_3)_4(H_2O)_9$ **(2a)**	12.44	15.54	2.05	3.11	7.65
$Ni_{20}(OH)_{40}Br_4(H_2O)_{15}$ **(2b)**	12.45	15.56	2.05	3.11	7.74
$Ni_{20}(OH)_{40}Cl_4(H_2O)_{15}$ **(2c)**	12.44	15.55	2.05	3.11	7.64
$Ni_{20}(OH)_{40}F_4(H_2O)_{15}$ **(2d)**	12.43	15.53	2.05	3.11	7.47
$Ni_{20}(OH)_{40}(OH)_4(H_2O)_{15}$ **(2e)**	12.43	15.53	2.05	3.11	7.46
$Ni_{20}(OH)_{40}(SO_4)_3(H_2O)_{10}$ **(2f)**	12.37	15.46	2.04	3.09	8.32
$Ni_{20}(OH)_{40}(CO_3)_3(H_2O)_{10}$ **(2g)**	12.36	15.46	2.04	3.09	7.31

Table 5. Simulated Structures of Al/Ni-LDHs (3) Models

	a (Å)	*b* (Å)	Ni−O (Å)	Al−O (Å)	O···O (Å)	interlayer distance (Å)
$Ni_{18}Al_6(OH)_{48}(NO_3)_6(H_2O)_{12}$ **(3a)**	12.25	18.39	2.05	1.91	3.06	8.05
$Ni_{18}Al_9(OH)_{48}Br_6(H_2O)_{18}$ **(3b)**	12.25	18.38	2.05	1.91	3.06	7.89
$Ni_{18}Al_6(OH)_{48}Cl_6(H_2O)_{18}$ **(3c)**	12.23	18.35	2.05	1.91	3.06	7.76
$Ni_{18}Al_6(OH)_{48}F_6(H_2O)_{18}$ **(3d)**	12.20	18.32	2.05	1.91	3.05	7.60
$Ni_{18}Al_6(OH)_{48}(OH)_6(H_2O)_{18}$ **(3e)**	12.21	18.32	2.05	1.91	3.05	7.60
$Ni_{18}Al_6(OH)_{48}(SO_4)_3(H_2O)_{12}$ **(3f)**	12.20	18.30	2.04	1.91	3.05	8.45
$Ni_{18}Al_6(OH)_{48}(CO_3)_3(H_2O)_{12}$ **(3g)**	12.19	18.29	2.04	1.91	3.05	7.53
$Ni_{12}Al_6(OH)_{36}(NO_3)_6(H_2O)_9$ **(3h)**	9.11	18.22	2.05	1.91	3.04	9.08
$Ni_{12}Al_6(OH)_{36}(SO_4)_3(H_2O)_{24}$ **(3i)**	9.12	18.24	2.05	1.91	3.04	10.05

(2c, 3c), F^- **(2d, 3d)**, and OH^- **(2e, 3e)**, and 2.04 Å in those containing divalent interlayer anions, CO_3^{2-} **(2f, 3f)** and SO_4^{2-} **(2g, 3g)**. Similarly, aluminum−oxygen bonds in Ni/Al-LDHs containing monovalent interlayer anions are slightly longer than those in Ni/Al-LDHs containing bivalent interlayer anions, and such a trend can also be observed for the O···O distance because of the larger electrostatics attractive force caused by bivalent anions.

D. Interlayer Structures of α-Ni(OH)$_2$ and Ni/Al LDHs. The interlayer separation is an important structural parameter for LDHs, and it can be experimentally determined by XRD. The interlayer spacing in α-$Ni(OH)_2$ (**2**) and Ni/Al-LDHs (**3**) depends on both the properties of interlayer anions and the number of interlayer water molecules, as illustrated in Figure 4. In general, interlayer anions with larger volume and/or more water molecules result in larger interlayer distances. In our simulations, the interlayer distances of α-$Ni(OH)_2$ (**2**) and Ni/Mg-LDHs (**3**) are in good agreement with previous experimental results. The interlayer distances of α-$Ni(OH)_2$ and Ni_3Al-LDHs containing NO_3^- are calculated to be 7.65 and 8.08 Å, correlating well with 7.56 and 7.89 Å from powder XRD data,[10] respectively. Our simulations have identified three possible packing modes, *Types 1−3*, for interlayer water molecules in α-$Ni(OH)_2$ (**2**) and Ni/Al-LDHs (**3**), which are shown in Figure 4.

McEwen has estimated the interlayer spacing for these three stacking configurations in α-$Ni(OH)_2$**,** taking the radius of a water molecule as 1.7 Å.[5] *Type 1* represents a small interlayer distance of around 7.6 Å (Figure 4a), where the interlayer water molecules are close packed and lie midway between the brucite-like sheets.[5] In *Type 2*, when the interlayer species have larger volume, the interlayer distance increases to around 8.0 Å. In the case of *Type 3*, expanded interlayer spacing of 10.5 Å permits a double water layer with two molecules thick. These situations are demonstrated in our simulations. First, the α-$Ni(OH)_2$ and Ni/Al-LDHs containing NO_3^- **(2a, 3a)**, Br^- **(2b, 3b)**, Cl^- **(2c, 3c)**, F^- **(2d, 3d)**, OH^- **(2e, 3e)**, and CO_3^{2-} **(2g, 3g)** adopt a packing structure of *Type 1*, in which the interlayer water molecules and anions are closely packed, parallel to hydroxide layers, and the interlayer spacing distances of α-$Ni(OH)_2$ are close to 7.6 Å (Figure 4a, Figures S1 and S2 in Supporting Information). It can be formed that the orientation of the C_2 axis of interlayer water molecules is parallel to the metal hydroxide sheets, consistent with a previous NMR study on an Mg/Al-LDH containing NO_3^-.[60] Another configuration was observed in Mg_3Al-LDH containing CO_3^{2-}, with the C_2 axes perpendicular to the sheets,[61] probably due to the different Mg/Al ratio. Second, the α-$Ni(OH)_2$ and Ni/Al-LDHs containing SO_4^{2-} **(2f, 3f)** exhibit the packing style of *Type 2* with water molecules slightly slanting between the metal hydroxide sheets (Figure 4b, Figures S1 and S2). Figure 5 shows the difference in slanting angles, ϕ, as defined by the orientation angles of H···H vectors of water molecules relative to the layers, in **3a** ($\phi = 0-20°$) and **3f** ($\phi = 0-40°$). So in **2f** and **3f**, some interlayer water molecules are oblique to the hydroxide layers, taking advantage of relatively large interlayer spaces (**2f**: 8.32 Å; **3f**: 8.45 Å). The Ni/Al-LDH containing SO_4^{2-} **(3i)** has the largest interlayer spacing distance of 10.05 Å, due to its larger interlayer water content compared to that in **3f**. It belongs to *Type 3*, in which two layers of water molecules are packed within the interlayer galleries (Figure 4c). This result also agrees with the reported

(60) Marcelin,G.; Stockhausen, N. J.; Post, J. F. M.; Schutzt, A. *J. Chem. Phys.* **1989**, *93*, 4646.
(61) van der Pol, A.; Mojet, B. L; van de Ven, E.; de Boer, E. *J. Phys. Chem.* **1994**, *98*, 4050.

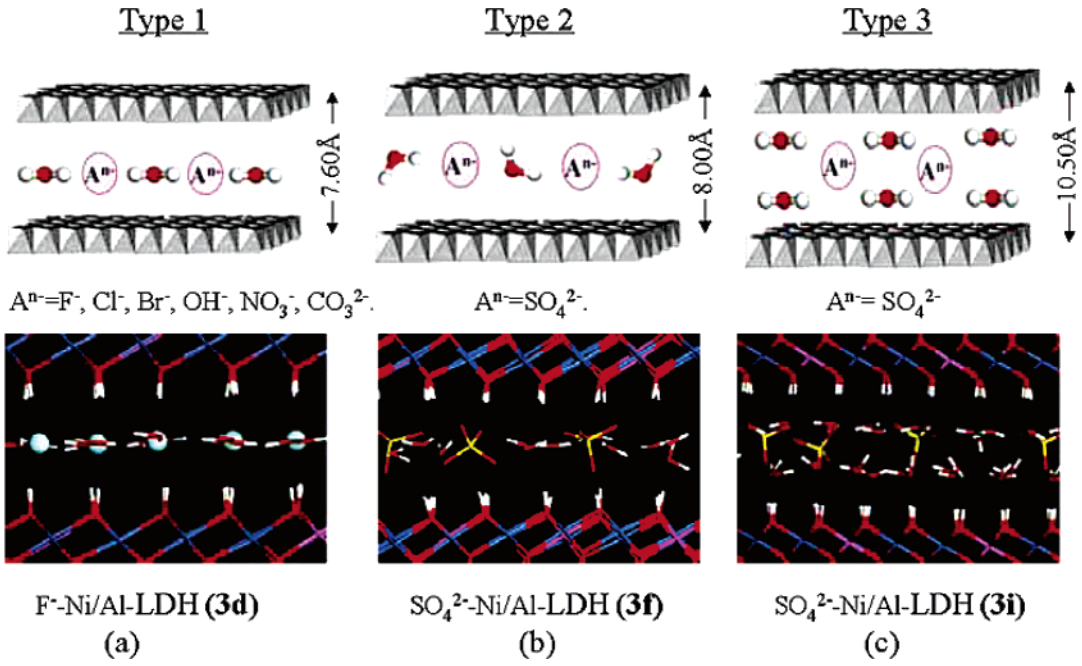

Figure 4. Possible packing styles of interlayer water molecules of α-Ni(OH)$_2$ **(2)** and Ni/Al-LDHs **(3)**. The snapshots obtained at 50 ps for (a) F$^-$−Ni/Al-LDH **(3d)**, (b) SO_4^{2-}−Ni/Al-LDH **(3f)**, and (c) SO_4^{2-}−Ni/Al-LDH **(3i)** are also given for illustration.

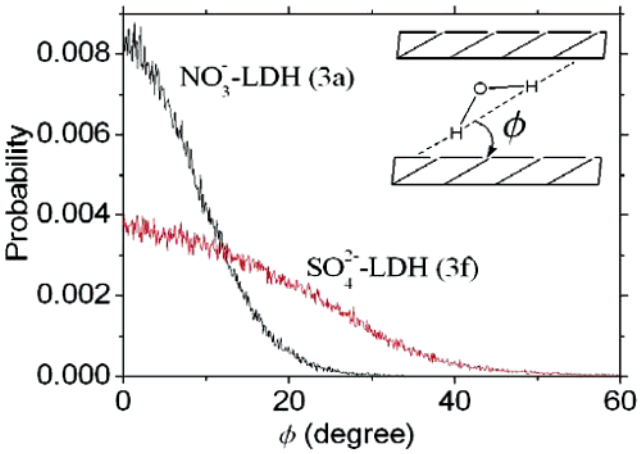

Figure 5. Distributions of slanting angles, *f*, between hydroxide layers and H···H vectors of interlayer molecules. The black line is the distribution of *f* in NO_3^-−Ni/Al-LDH **(3a)**, and the red one corresponds to that in SO_4^{2-}−Ni/Al-LDH **(3f)**.

XRD study of SO_4^{2-}−Fe(II−III)-LDHs.[34]

An abrupt structural transformation in NO_3^-−Mg/Al-LDHs has been detected when varying the Mg/Al ratio.[33] It was reported that when the Mg/Al ratio decreases from 3 to 2, the interlayer spacing increases from 8.08 to 8.95 Å.[33] Three models have been proposed to explain this transformation, as shown in Figure 6a.[33] To better understand the influence of Ni/Al ratio, a MD simulation is performed on a NO_3^-−Ni/Al-LDH model, **3h**, with 2:1 Ni/Al ratio.

Figure 6b compares the distribution of tilt angles, θ, of NO_3^- plane with respect to metal hydroxide sheets (as defined in Figure 6a) between NO_3^-−Ni/Al-LDH **(3a)** and NO_3^-−Ni/Al-LDH **(3h)** models with Ni/Al ratios of 3 and 2, respectively. The tilt angles in **3a** are mostly populated around 15°, while those in **3h** have a much wider distribution ranging from 40° to 90°. It can be deduced that the NO_3^- anions are nearly parallel to the hydroxide in **3a** but slanting in **3h**, corresponding to the flat- and tilt-lying models, respectively (see Figure 6). At the same time, the flat-lying style of interlayer water molecules in **3a** corresponds to the closely packed *Type 1* as shown in Figure 4a, while tilt-lying style in **3h** belongs to *Type 2* in Figure 4b. The packing density of NO_3^- in **3h** is much larger than that in **3a**. Thus, the NO_3^- anions stack in a tilted or even vertical arrangement with respect to the hydroxide layers in **3h** in order to decrease the area they occupy on the surface of hydroxide layers. The stick-lying style was not found during our MD simulations, although the possibility of its existence has been suggested on the basis of experimental evidence.[33,62]

LDHs containing SO_4^{2-} are also known to have two possible interlayer arrangements with very different interlayer spacings, depending on the amount of interlayer water molecules. Experimentally, two forms were able to be interconverted by varying the relative humidity in which the LDH sample was stored.[63] Therefore, we have investigated two models of SO_4^{2-}−Ni/Al-LDHs **(3f)** and **(3i)**, which have different anion concentrations and interlayer water contents. One important structural parameter is the orientation of the SO_4^{2-} tetrahedra relative to the layers. The orientation parameter (ω) for the SO_4^{2-} tetrahedron is defined as the maximum angle between one C_3 axis of the SO_4^{2-} tetrahedron and the hydroxide layers, as shown in Figure 7a.

The distributions of the orientation angle ω in SO_4^{2-}−Ni/Al-LDHs **(3f)** and **(3i)** are shown in Figure 7. The value of ω in **3f** populates in the range of 35°−45°, indicating that, in this configuration, each SO_4^{2-} tetrahedron has one C_2 axis perpendicular to the hydroxide layers, which is consistent with experimental observations on anhydrous LDHs containing SO_4^{2-}.[64] In contrast, in **3i**, there are two peaks of orientation parameters, at 35°−55° and 65°−90°, respectively. This suggests that there are two orientations

(62) Gago, S.; Pillinger, M.; Valente, A. A.; Santos, T. M.; Rocha J.; Gonçalves, I. S. *Inorg. Chem.* **2004**, *43*, 5422.
(63) Bish, D. L. *Bull. Minéral.* **1980**, *103*, 170.

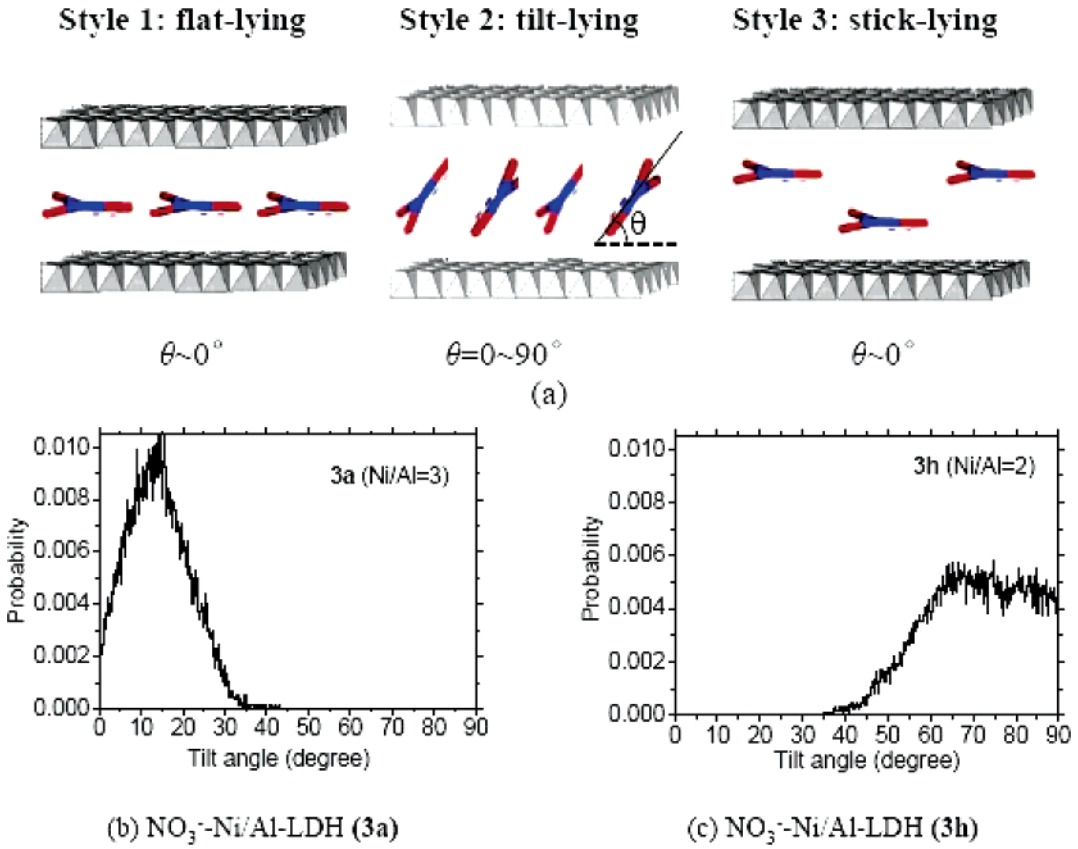

Figure 6. Possible stacking styles regarding the arrangement of nitrate anions in NO_3^-−Ni/Al-LDHs are given in (a). Distributions of tilt angles θ of NO_3 plane with respect to hydroxide sheets in (b) NO_3^-−Ni/Al-LDH with Ni/Al = 3 **(3a)** and (c) NO_3^-−Ni/Al-LDH with a ratio of 2 **(3h)** models.

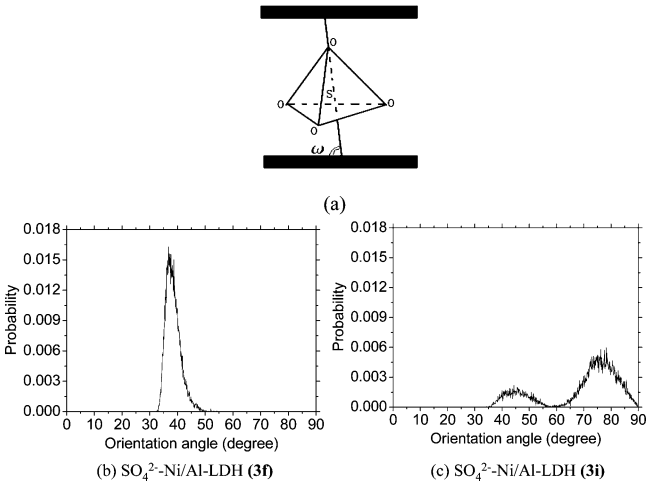

Figure 7. Orientation parameter (ω) for the SO_4^{2-} tetrahedron is defined as the largest angle between c3 axes of SO_4^{2-} tetrahedron and hydroxide layers, as shown in (a). Here are distributions of orientation parameter ω of (b) SO_4^{2-}−Ni/Al-LDH **(3f)** containing 13 water molecules per layer and (c) SO_4^{2-}−Ni/Al-LDH **(3i)** containing 30 water molecules per layer.

for the SO_4^{2-} tetrahedra, with a minority having similar geometry to that in **3f** (ω = 35−45°), but the majority having their C_3 axes perpendicular to the hydroxide layers (ω = 65−90°). The arrangement of interlayer water molecules in **3i** takes *Type 3* in Figure 4c, and the interlayer distance in **3i** (10.05 Å) is larger than that in **3f** (8.45 Å). It is interesting to recall that the experimental interlayer distance is 11.10 Å for Fe(II−III) layered double hydroxysulfate green rust two[34] and 8.6−8.7 Å for ordinary Mg/Al LDHs containing SO_4^{2-},[65,66] which are quite close to the calculated values for SO_4^{2-}−Ni/Al-LDH **(3i)** and **(3f)**, respectively. This reveals that the nature and amount of both interlayer anions and water molecules play important roles in determining the packing styles in mixed metal layered materials.

E. Binding Energies of Anions in α-Ni(OH)$_2$ and Ni/Al-LDHs. The ion exchange method is often used to synthesize LDHs containing a variety of anions. The abilities of anions to bind with LDHs vary considerably, with the affinity generally decreasing in the order of $CO_3^{2-} > SO_4^{2-} > OH^- > F^- > Cl^- > Br^- > NO_3^-$.[3,13] The binding energy between the metal hydroxide layers and interlayer anions may provide a clue to understanding the relative order of the exchange ease of anions. Here, the relative binding energy of anions in α-Ni(OH)$_2$ is defined as below

$$\Delta U_B(A^{n-}) = \frac{\langle U_{\alpha-Ni(OH)_2}\rangle - \langle U_{NO_3^-\alpha-Ni(OH)_2}\rangle - N_w\langle U_{H_2O}\rangle - N_A\langle U_A\rangle}{N_A} \quad (3)$$

where $\langle U_{\alpha-Ni(OH)_2}\rangle$ is the average potential energy of the α-Ni(OH)$_2$ **(2)** model with interlayer anion A^{n-}. Because we just want to know the relative binding energies of α-Ni(OH)$_2$ **(2)** with various interlayer anions, and the α-Ni(OH)$_2$ containing NO_3^- **(2a)** has the smallest binding energy, the average potential energy of **2a**, $\langle U_{NO_3^-\alpha-Ni(OH)_2}\rangle$, is taken as

(64) Hou, X.; Bish, D. L.; Wang, S.-L.; Johnston, C. T.; Kirkpatrick, R. J. *Am. Mineral.* **2003**, *88*, 167.
(65) Miyata, S.; Okada, A. *Clays Clay Miner.* **1977**, *25*, 14.
(66) Hansen, H. C. B.; Taylor, R. M. *Clay Miner.* **1991**, *26*, 311.

Table 6. Potential Energies and Relative Binding Energies of α-Ni(OH)$_2$ (2) and Ni/Al-LDHs (3)

LDH model	interlayer anion	potential energy (kcal/ mol)	binding energy (kcal/ mol)
β-Ni(OH)$_2$ **(1)**		−51526.24	
α-Ni(OH)$_2$ **(2)**			
2a	NO_3^-	−56341.18	0
2b	Br^-	−56736.69	−32.95
2c	Cl^-	−56860.39	−43.26
2d	F^-	−57071.44	−60.85
2e	OH^-	−57166.58	−68.78
2f	SO_4^{2-}	−60332.70	−577.25
2g	CO_3^{2-}	−60918.32	−652.68
Ni/Al-LDHs **(3)**			
3a	NO_3^-	−70832.36	0
3b	Br^-	−71403.58	−31.73
3c	Cl^-	−71615.95	−43.53
3d	F^-	−71946.32	−61.89
3e	OH^-	−72073.14	−68.93
3f	SO_4^{2-}	−71705.52	−97.02
3g	CO_3^{2-}	−72207.35	−163.15

a reference. $\langle U_{H_2O}\rangle$ and $\langle U_A\rangle$ are respectively the average potential energies of a single water molecule and anion. N_w and N_A are the number of water molecules and interlayer anions, respectively. From this definition, the relative binding energy mainly consists of two components, the interaction energy between interlayer molecules and the interaction energy between interlayer molecules and hydroxide layers.

Since the Ni/Al-LDH containing NO_3^- **(3a)** has the smallest binding energy, $\Delta U_B(NO_3^-)$ is also set to be the zero-point of relative binding energies in Ni/ Al-LDHs **(3)**. Hence, the relative binding energy of anions in Ni/Al-LDHs can be calculated from eq 4

$$\Delta U_B(A^{n-}) = \frac{\langle U_{LDH}\rangle - \langle U_{NO_3^-\text{-}LDH}\rangle - N_w\langle U_{H_2O}\rangle - N_A\langle U_A\rangle}{N_A} \quad (4)$$

where $\langle U_{LDH}\rangle$ is the average potential energy of Ni/Al-LDHs **(3)**, and $\langle U_{NO_3^-\text{-}LDH}\rangle$ is the average potential of Ni/Al-LDH containing nitrate anions **(3a)**.

Potential energies and relative binding energies of α-Ni(OH)$_2$ **(2)** and Ni/Al-LDHs **(3)** are listed in Table 6. Clearly, the calculated relative binding energies, shown in Figure 8, have the same order as the relative affinity concluded from ion exchange experiments.[3,13] For α-Ni(OH)$_2$ **(2)**, we obtain the order of $CO_3^{2-} > SO_4^{2-} > OH^- > F^- > Cl^- > Br^- > NO_3^-$ in relative binding energy (Figure 8a), and for Ni/Al-LDHs **(3)** we have $CO_3^{2-} > SO_4^{2-} > OH^- > F^- > Cl^- > Br^- > NO_3^-$ (Figure 8b). The nitrate anion has the smallest

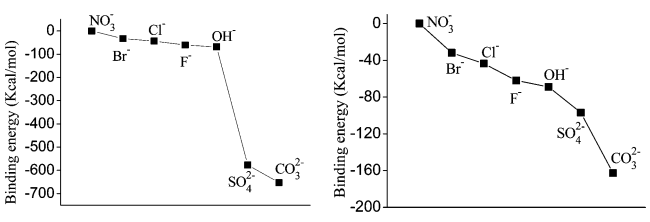

(a) α –Ni(OH)$_2$ (b) Ni/Al-LDHs

Figure 8. Relative binding energies of different interlayer anions in (a) α-Ni(OH)$_2$ **(2)** and (b) Ni/Al-LDHs **(3)**. The zero points of binding energy are −56341.18 and −70832.36 kcal/mol for α-Ni(OH)$_2$ and Ni/AL-LDHs, respectively.

Table 7. Potential Energies of NO_3^-−α-Ni(OH)$_2$ (2a) Obtained by Using Atomic Partial Charges of NO_3^- from Various Methods

	Mulliken	NBO	CHELPG
partial charge of N	−0.052	0.686	1.109
partial charge of O	−0.316	−0.561	−0.703
potential energy (kcal/mol)	−56730.17	−56717.47	−56728.30

binding energy with the hydroxide layers, consistent with the fact that the nitrate anion is most readily exchanged by other anions from the interlayer.[3] In contrast, CO_3^{2-} has the largest binding energy, and since CO_2 is present in the atmosphere, it is not surprising that LDHs containing other anions are readily contaminated by CO_2.[3]

To take a closer look at the relative binding energies, a further analysis is performed. It can be found that the binding energy mainly comes from the Coulombic interaction, which contributes more than 90% of the potential energy, as shown in eq 5

$$E_{Coulomb} = \sum \frac{\epsilon}{4\pi}\frac{q_i q_j}{r^2} \quad (5)$$

where q_i and q_j denote the charges of atoms i and j, respectively, r is the interatomic distance between atoms i and j, and ϵ is the dielectric constant. Thus, larger atomic charges and smaller interatomic distances will yield larger binding energies.

Obviously, divalent anions have larger net charges than monovalent anions, so relative binding energies of LDHs containing the former are much larger than those containing the latter. Thus, the LDHs containing CO_3^{2-} **(2g, 3g)** and SO_4^{2-} **(2f, 3f)** have larger binding energies than other LDHs. A comparison of the potential energies of the NO_3^-−α-Ni(OH)$_2$ **(2a)** model, obtained by using the atomic partial charges of NO_3^- from Mulliken,[67] NBO,[47] and CHELPG[68−70] population analysis on the basis of DFT (B3LYP/6-31+G(d)) calculations is shown in Table 7. Although there are distinct differences in atomic partial charges for NO_3^- obtained by using the various methods, the differences in potential energies are insignificant. This implies that partial atomic charge plays a less important role than what might have been expected.

It is meaningful to correlate the second important parameter, the interatomic distance r in eq 5 with relative binding energies of LDHs containing F^- **(2d, 3d)**, Cl^- **(2c, 3c),** and Br^- **(2b, 3b)** because they have similar structures and atomic charges. The van der Waals radii of these anions increase in the order F^- (1.47 Å) < Cl^- (1.76 Å) < Br^- (1.85 Å),[71] and the interlayer spacing follows the same order. Therefore, it is understandable that the binding energies vary in a sequence of F^- (**3d**: −31.73 kcal/mol) > Cl^- (**3c**: −43.53 kcal/mol) > Br^- (**3b**: −61.89 kcal/mol).

It must be mentioned that in actual ion exchange reaction of LDHs, entropy effects (ΔS) are also important, especially for large organic guest anions. Some previous calorimetric

(67) Mulliken, R. S. *J. Chem. Phys.* **1955**, *23*, 1833.
(68) Chirlian, L. E.; Francl, M. M. *J. Comput. Chem.* **1987**, *8*, 894.
(69) Breneman, C. M.; Wiberg, K. B. *J. Comput. Chem.* **1990**, *11*, 361.
(70) Francl, M. M.; Carey, C.; Chirlian, L. E.; Gange, D. M. *J. Comput. Chem.* **1996**, *17*, 367.
(71) Bondi, A. *J. Phys. Chem.* **1964**, *68*, 441.

experiments have been performed in order to study the anion exchange in Zn/Al-LDHs.[72−74] It has been suggested that the exchange processes appear to be entropy-driven, but that the selectivity is controlled by the enthalpic contribution.[73] Unfortunately, the entropy effect is difficult to evaluate using current theoretical models. The relative binding energy is still a useful tool to interpret experimental phenomena.

Conclusions

Molecular dynamics (MD) simulations of β-$Ni(OH)_2$ **(1)**, α-$Ni(OH)_2$ **(2)**, and Ni/Al-LDHs **(3)** have been performed in order to study the structure and binding energy of the materials containing various anions, viz. CO_3^{2-}, SO_4^{2-}, OH^-, F^-, Cl^-, Br^-, and NO_3^-. A modified force field based on cff91 is suggested and new parameters for describing O−Ni−O angle bending and Ni−O bond stretching in nickel hydroxides are introduced, and NBO analysis of partial charges of various interlayer anions is performed.

The models presented here are useful in rationalizing the structure of the metal-hydroxide sheets and arrangement of interlayer anions in α-$Ni(OH)_2$, which have been the subject of different interpretations in the literature. The structural properties, such as metal−oxygen bond lengths, size of unit cell, and interlayer distances in β-$Ni(OH)_2$, α-$Ni(OH)_2$, and Ni/Al-LDHs obtained from our simulations, are in good agreement with experimental data. Many other details of the structure of these compounds, which are difficult to observe experimentally, are also presented. The packing modes of interlayer water molecules are studied, supporting the previous hypothesis.[5] The interlayer water molecules in α-$Ni(OH)_2$, and Ni/Al-LDHs containing NO_3^- **(2a, 3a)**, Br^- **(2b, 3b)**, Cl^- **(2c, 3c)**, F^- **(2d, 3d)**, OH^- **(2e, 3e)**, and CO_3^{2-} **(2g, 3g)**, are closely packed. The α-$Ni(OH)_2$ and Ni/Al-LDH containing SO_4^{2-} **(2f, 3f)** have less compact arrangements of water molecules in the interlayer space, while in Ni/Al-LDH containing SO_4^{2-} **(3i)** with larger water content, there are two layers of water molecules within the interlayer space. The different packing modes in Ni/Al-LDHs containing NO_3^- and SO_4^{2-}, arising from the variation in Ni/Al ratio and water content, are also investigated.

The positive value of the "hydration energy" of β-$Ni(OH)_2$ is consistent with the observed anhydrous nature of β-$Ni(OH)_2$. The relative binding energies calculated by our MD simulations can rationalize the relative affinity of various anions in ion exchange experiments, $CO_3^{2-} > SO_4^{2-} > OH^- > F^- > Cl^- > Br^- > NO_3^-$. Coulombic interaction is the major contribution to the potential energies. The net charge and van der Waals radius of interlayer anion both significantly affect the binding energy, and the amount of interlayer water molecules also plays an important role in binding energy, especially for those containing large organic anions.

Further improvement in the force field will be explored in our future work since the present force field may result in too rigid LDH layers to observe the large distortion of LDH sheets caused by interlayer molecules and anions, as reported by Wang et al.[16] The possible coordinative interaction between interlayer anions such as NO_3^- and metal hydroxide layers as well as entropy effects in the process of ion exchange will also be taken into account in our future work.

Acknowledgment. This work was supported by the National Basic Research Program (No. 2004CB720602), the National Science Foundation of China (Nos. 20420150034, 90303020, 20433020, 20573050), and NCET-05-0442 from the Ministry of Education.

Supporting Information Available: Figures S1 and S2 show the snapshots of α-$Ni(OH)_2$ **(2)** and Ni/Al-LDHs **(3)** containing various anions during the MD simulations at 50 ps. Table S1 presents the thermodynamic and structural properties of water obtained from a MD simulation on liquid water. This material is available free of charge via the Internet at http://pubs.acs.org.

CM060867H

(72) Israëli, Y.; Taviot-Guého, C.; Besse, J.-P.; Morel, J.-P.; Morel-Desrosiers, N. *J. Chem. Soc., Dalton Trans.* **2000**, 791.
(73) Morel-Desrosiers, N.; Pisson, J.; Israëli, Y.; Taviot-Guého, C.; Besse, J.-P.; Morel, J.-P. *J. Mater. Chem.* **2003**, *13*, 2582.
(74) Bravo-Suárez, J. J.; Páez-Mozo, E. A.; Oyama, S. T. *Quim. Nova* **2004**, *4*, 574.